Energy efficient torque vectoring control

GRUBER, P, SORNIOTTI, A, LENZO, Basilio <http://orcid.org/0000-0002-8520-7953>, DE FILIPPIS, G and FALLAH, S

Published version

GRUBER, P, SORNIOTTI, A, LENZO, Basilio, DE FILIPPIS, G and FALLAH, S (2016). Energy efficient torque vectoring control. In: AVEC '16 : 13th International Symposium on Advanced Vehicle Control, Munich, Germany, 13-16 September, 2016. CRC Press. (In Press)

Energy efficient torque vectoring control

P. Gruber, A. Sorniotti, B. Lenzo, G. De Filippis, S. Fallah
University of Surrey, Guildford, United Kingdom

ABSTRACT: Tire forces are at the heart of the dynamic qualities of vehicles. With the advent of electric vehicles the precise and accurate control of the traction and braking forces at the individual wheel becomes a possibility and a reality outside test labs and virtual proving grounds. Benefits of individual wheel torque control, or torque-vectoring, in terms of vehicle dynamics behavior have been well documented in the literature. However, very few studies exist which analyze the individual wheel torque control integrated with vehicle efficiency considerations. This paper focuses on this aspect and discusses the possibilities and benefits of integrated, energy efficient torque vectoring control. Experiments with a four-wheel-drive electric vehicle show that considerable energy savings can be achieved by considering drivetrain and tire power losses through energy efficient torque vectoring control.

1 INTRODUCTION

Typically, by generating different traction/braking forces on the left and right hand sides of a vehicle, a torque-vectoring (TV) controller induces a yaw moment that directly influences the vehicle handling qualities. With the introduction of electric vehicles with multiple motors, the tire forces can be controlled in a precise and accurate way and, importantly, at each wheel of the car. As a result, the system becomes overactuated and the asymmetric torque distribution between the vehicle sides can be achieved in infinite ways. This configuration opens up several development avenues to substantially alter the vehicle characteristics both in terms of cornering behavior and energy efficiency, without changing the mechanical setup. For instance, a large body of literature discusses the possible vehicle dynamics improvements, including active safety and fun-to-drive aspects, that can be achieved through TV control (e.g., Jonasson et al., 2011, Kang et al., 2011), see section 2.1. In recent years, research activities have been extended to explore individual wheel torque control integrated with vehicle efficiency considerations (e.g., Wang et al., 2011, De Novellis et al., 2013, Chen & Wang, 2014, Fujimoto & Harada, 2015), see section 2.2.

This article is an account of the possibilities and benefits of integrated, energy efficient torque vectoring control by presenting and discussing results obtained with the fully electric vehicle (EV) demonstrator of the European Union FP7 projects E-VECTOORC (www.e-vectoorc.eu) and iCOMPOSE (www.i-compose.eu). The EV is a prototype Range Rover Evoque equipped with four identical on-board electric drivetrains, each of them comprising a switched reluctance electric motor (75 kW peak power, 35 kW nominal power, and 80 Nm nominal torque), a single-speed transmission system (10.56:1 gear ratio), constant velocity joints, and a half-shaft (Figs 1,2).

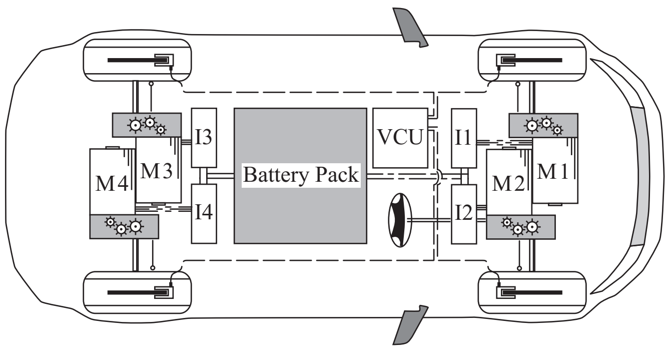

Figure 1. Schematic of the four-wheel-drive architecture of the vehicle demonstrator, where M1-M4 = switched reluctance motor; I1-I4 = inverter; and VCU = vehicle control unit.

Figure 2. Experimental testing of the vehicle demonstrator on the rolling road and at the Lommel proving ground (Belgium).

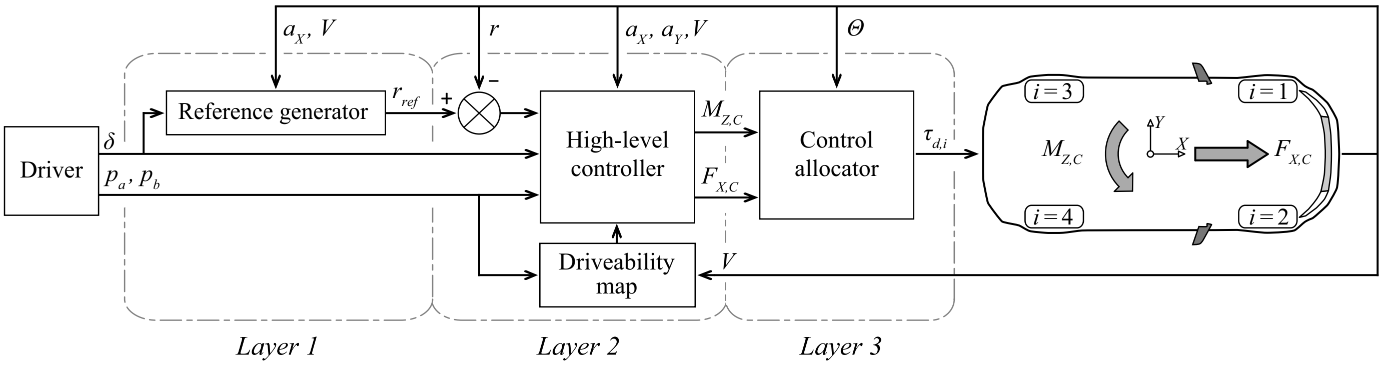

Figure 3. Modular structure of vehicle control system comprising three main layers.

2 TORQUE VECTORING CONTROL

2.1 *Control structure*

To allow easy implementation of the developed vehicle controllers, a modular control architecture has been adopted consisting of three main layers (Fig. 3):

1 In Layer 1, a reference generator defines the target values of the vehicle states (e.g., the reference yaw rate, r_{ref}) based on the driver inputs (steering wheel angle, δ, accelerator and brake pedal positions, p_a and p_b), and the measured/estimated states (e.g., vehicle speed, V, and longitudinal/lateral acceleration, $a_{X/Y}$).

2 A high-level controller is implemented in Layer 2 to determine the overall traction/braking force and yaw moment demands, $F_{X,C}$ and $M_{Z,C}$, to achieve the reference values of the vehicle states.

3 The reference torques, $\tau_{d,i}$, for the individual wheels corresponding to the values $F_{X,C}$ and $M_{Z,C}$ are computed in the Layer 3 by a low-level controller, i.e., the Control allocator. $\boldsymbol{\Theta}$ is the vector of parameters (e.g., V) required for the calculation of the optimal wheel torque distribution.

For the experimental tests, the developed vehicle controllers were implemented on a dSPACE AutoBox system (VCU in Fig. 2) and the signals were transmitted through CAN.

2.2 *Vehicle dynamics enhancement*

Torque-vectoring allows enhancing the handling qualities of a vehicle well beyond the capabilities achievable with current conventional stability control systems (van Zanten et al., 1995) as the controller interventions can be seamlessly and continuously generated without variation of the net traction force (De Novellis et al., 2015a). In particular, the controlled distribution of the traction and braking torques among the wheels allows the design of the steady-state and transient cornering responses of the vehicle (De Novellis et al., 2012) and, thus, the creation of fundamentally different driving modes. For example, a model-based design procedure is used in De Novellis et al. (2015b) to define sets of vehicle understeer characteristics at different longitudinal accelerations and the corresponding reference yaw rates (implemented in Layer 1, section 2.1.) that yield a sporty vehicle cornering behavior. That is, a Sport mode was designed to reduce the understeer gradient, extend the region of linear vehicle operation, and significantly increase the maximum lateral acceleration compared to the passive vehicle (Fig. 4a). The active safety benefits of the TV controller during highly-transient maneuvers are highlighted by the time history of the measured yaw rate during an extreme step steer test. Figure 4b shows that the controller allows a considerable reduction of the yaw rate oscillations and settling time. Hence, the vehicle behavior is more consistent and predictable so that driving in extreme conditions becomes easier.

In order to exploit the full benefits of TV control in a safe way in all possible driving conditions the road friction conditions need to be known or, at least, reasonably well estimated. Unfortunately, this is not a trivial task. As an alternative, the torque-vectoring algorithm can be coupled with sideslip control to create a more robust controller that shows consistent and safe performance nearly

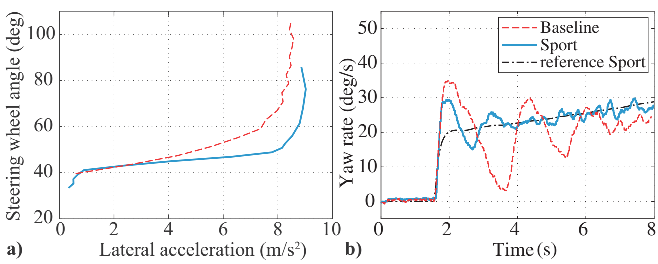

Figure 4. a) experimental understeer characteristics for the passive vehicle ("Baseline") and the active vehicle in "Sport" mode achieved during skid-pad tests. b) yaw rate response of the passive vehicle and the controlled vehicle (including reference yaw rate) during step steer tests with 100 deg of steering wheel angle amplitude at 100 km/h.

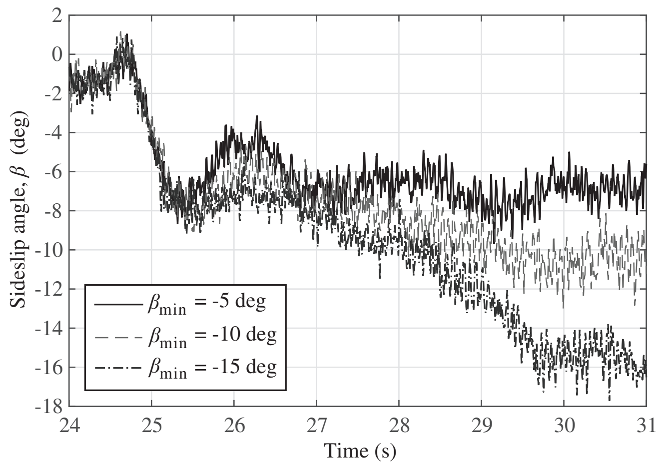

Figure 5. Vehicle sideslip angle during step steer tests with 100 deg of steering wheel angle amplitude at 90 km/h with three different predefined sideslip limits β_{min} (Lu et al., 2016).

independent of the prevailing friction conditions (Lu et al., 2016). Also, the concurrent yaw rate and sideslip controller allows the vehicle to operate at specified sideslip angles to enhance active safety (Fig. 5). Conversely, the controller could be used to create a drift mode to improve the fun-to-drive aspect.

2.3 *Energy-efficiency improvement*

Owing to the actuation redundancy of EVs with multiple motors, TV control can be used to minimize the overall energy consumption without compromising vehicle dynamics characteristics. In particular, power losses in the drivetrain and due to tire slips (which become significant at high acceleration levels) are major sources of energy consumption that can be influenced by the individual wheel torque control (Tjønnas et al., 2010, Chen & Wang, 2012, Pennycott et al., 2014). Considering the capabilities of the TV controller, the energy-efficiency can be improved in two ways:

- by distributing the traction/braking force and yaw moment demands of the high-level controller (section 2.1, Layer 2) among the wheels according to specific energy efficient control allocation (CA) strategies (section 2.1, Layer 3), see section 3.
- by defining reference understeer characteristics (section 2.1, Layer 1) that minimize energy losses, provided that vehicle handling behavior may be influenced, see section 4.

The combination of both ways is possible and should maximize the energy savings benefits of torque-vectoring control.

3 ENERGY EFFICIENT CONTROL ALLOCATION

The energy efficient CA strategy implemented on the case study EV was developed based on measurements of the drivetrain power losses obtained on a rolling road facility. The power losses were determined from the difference between the measured electrical power at the inverter and the measured mechanical power at the roller of the test bench so that the results include the losses in the electric motor drive, mechanical transmission, tire rolling resistance and tire slip on the roller. Figure 6 shows that the drivetrain power loss characteristics are strictly monotonically increasing functions of wheel torque with a single inflection point and vary with vehicle speed. Based on this observation, a simple, computationally efficient torque distribution strategy for energy minimization is possible.

By assuming small steering angles and considering the basic vehicle geometry, the wheel torque distribution problem can be simplified by treating the two vehicle sides independently (Pennycott et al., 2014). That is, the torque demands corresponding to $F_{X,C}$ and $M_{Z,C}$ (section 2.1, Layer 2) for the left and right hand sides of the vehicle are given by:

$$\tau_{d,L/R} = \frac{1}{2}\left(F_X^C \mp \frac{M_Z^C}{d} \right) R \tag{1}$$

where d = half-track; and R = the wheel radius.

Using Equation (1), the developed energy efficient CA strategy (see details in Dizqah et al., 2016) employs a single drivetrain on each side of the vehicle when the respective torque demand on the left/right vehicle side ($\tau_{d,L/R}$) is lower than a specified switching value $\tau_{d,SW}$. Conversely, if the side torque demand is greater than $\tau_{d,SW}$ an even front-to-rear torque ratio on the particular side is

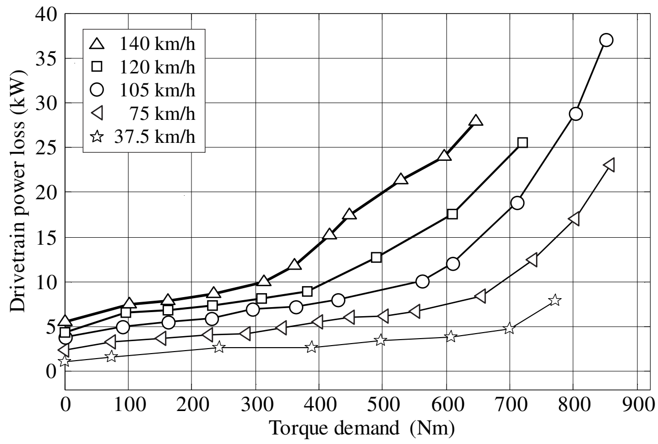

Figure 6. Measured power loss characteristics of a single electric drivetrain of the case study EV against torque demand at different vehicle speeds.

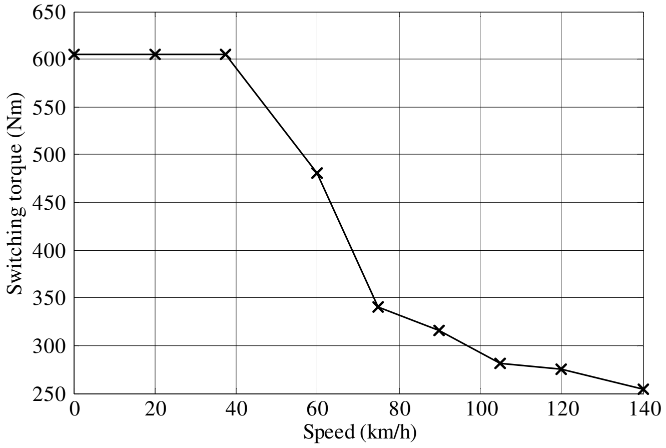

Figure 7. Switching torque for one vehicle side at different vehicle speeds.

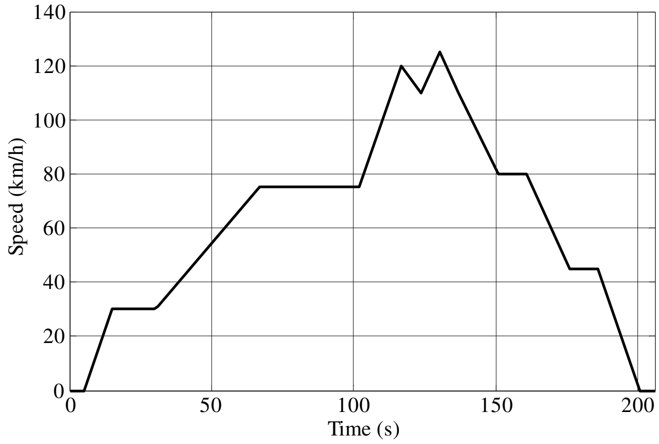

Figure 8. Speed profile of the SDDC.

used. To guard against drivability issues, the transition between the two torque distribution cases is smoothened with a sigmoid function.

The switching torque (Fig. 7) can be obtained offline by considering that the drivetrains of the case study EV have equal power losses P_{loss}. Then, $\tau_{d,SW}$ is found from the condition when the power loss of using only a single drivetrain is equal to the power loss of using an even distribution:

$$P_{loss}\,(\tau_{d,SW}, \boldsymbol{\Theta}) + P_{loss}\,(0, \boldsymbol{\Theta}) = 2P_{loss}\,(0.5\,\tau_{d,SW}, \boldsymbol{\Theta}) \tag{2}$$

The CA was experimentally tested on the vehicle demonstrator by completing different driving cycles on the rolling road and comparing the results with tests of the EV set up with either front-wheel-drive (Single Axle, SA) or four-wheel-drive (Even Distribution, ED) with constant 50:50 front-to-rear wheel torque distribution. The tested driving cycles included the New European Driving Cycle (NEDC) to simulate low to medium driving loads, and the Extra Urban Driving Cycle (EUDC) run with an emulated uphill constant road slope of 8% to replicate medium to high driving loads. For both driving cycles, the CA strategy yields the lowest energy consumption, see Table 1. In terms of the NEDC, the potential energy improvement of the CA is rather small (<1%) with respect to the SA mode, whereas substantial improvements (>2.9%) are achieved compared to the ED mode.

Table 1. Energy consumption along driving cycles.

Driving cycle	Energy consumption (kWh)			CA w.r.t. (%)	
	SA	ED	CA	SA	ED
NEDC	2.932	3.031	2.923	0.31	3.56
EUDC, 8% slope	5.838	5.739	5.716	2.09	0.40
SDDC	1.136	1.141	1.103	2.90	3.33

This behavior can primarily be ascribed to the relatively low drive torque required during the NEDC compared to the motor torque available on the case study EV, so that $\tau_{d,L/R} < \tau_{d,SW}$ is often true and the SA mode is close to being the most efficient torque distribution. This observation is confirmed by the greater energy savings achieved relative to the ED mode, and by the reversed trend for the EUDC with 8% slope, which requires a greater drive torque. In other words, an electric vehicle with less powerful drivetrains would show benefits more clearly in the two driving cycles. Thus, to emphasize the effect of the CA on energy consumption, a new driving cycle was created, it is called the Surrey Designed Driving Cycle (SDDC), see Figure 8. Over the SDDC, the CA algorithm is significantly better than the SA and ED modes, improving energy efficiency by 2.9% and 3.3%, respectively.

The concept of the simple, yet effective CA formulation is also valid during cornering and allows the car to operated with 2, 3 or 4 active motors. Tests of running the car at constant radius and velocity on a skid-pad showed energy consumption improvements of up to ~4% compared to the ED mode.

4 ENERGY EFFICIENT REFERENCE UNDERSTEER CHARACTERISTIC

To study the influence of understeer characteristics on energy consumption, experimental skid-pad tests (60 m radius) were carried out with the EV at four lateral accelerations (a_Y: ~2, 4, 6 and 8 m/s^2) and different handling settings, while the overall drivetrain power P was calculated from the product of the voltage and current measured at the battery. The EV handling settings were achieved with an even front-to-rear torque distribution on each vehicle side and by changing the yaw moment demand of the TV controller. In this way, the EV was run with eleven different understeer characteristics –

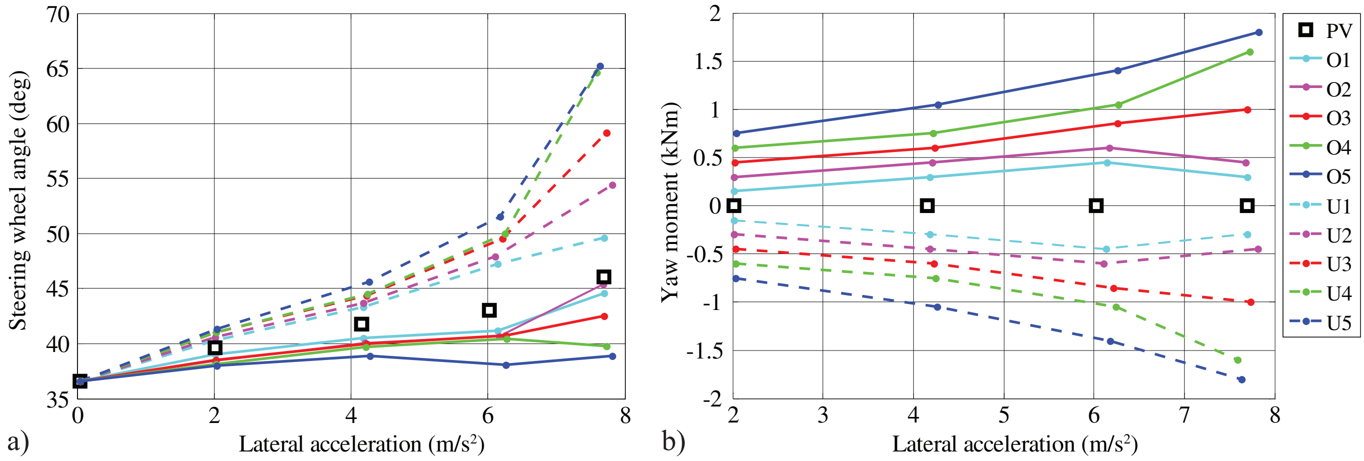

Figure 9. a) The experimentally measured understeer characteristics with different reference yaw moment settings. b) Reference yaw moment as a function of lateral acceleration for different understeer characteristics. The open black squares indicate the passive vehicle.

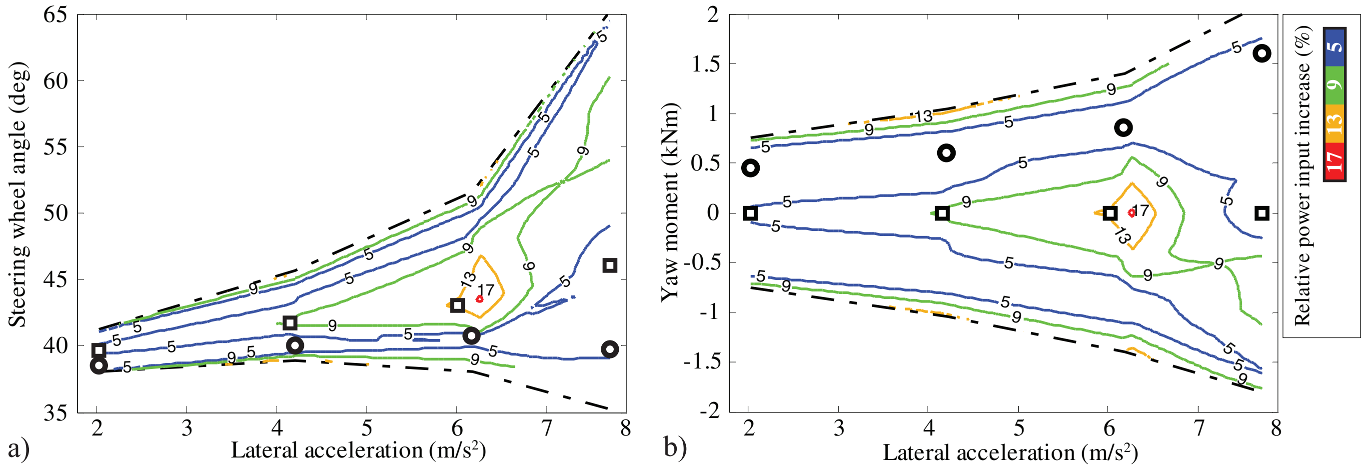

Figure 10. a) Map of understeer characteristics with iso-contour lines of relative drivetrain power increase with respect to the vehicle with the optimal understeer characteristic (indicated by black open circles). The passive vehicle understeer characteristic is shown by the black open squares and the boundaries of the measured region are indicated by the dash-dotted lines. b) Map of yaw moments with iso-contour lines of relative drivetrain power increase with respect to vehicle with optimal understeer characteristic. The optimum yaw moment is indicated by black open circles. The passive vehicle yaw moment is shown by the black open squares and the boundaries of the measured region are indicated by the dash-dotted lines.

one of the passive vehicle (denoted as PV), five characteristics with progressively increasing understeer (denoted as U1 to U5) and five characteristics with progressively decreasing understeer (denoted as O1 to O5) with respect to the passive vehicle (Fig. 9a). The yaw moments corresponding to the different understeer characteristics are shown in Figure 9b. Positive yaw moments yield a destabilizing control action (reducing understeer) and negative yaw moments generate a stabilizing effect (increasing understeer).

For ease of comparison, the measured drivetrain power is expressed relative to the power required by the vehicle set up with the most energy efficient understeer characteristic, which is given by the steering wheel angle that minimizes P for a particular lateral acceleration.

As indicated by Figure 10a, the optimal handling characteristic is achieved by reducing understeer compared to the passive vehicle. In particular, the most energy efficient cornering behavior is close to neutral steering, which is typically associated with sports car characteristics and, thus, can be assumed to also enhance active safety and fun-to-drive aspects (see section 2.2). Over the measured lateral acceleration range, the optimal understeer characteristic allows energy savings of up to ~11% compared to the passive vehicle. This potential saving is considerably greater than the improvements achievable with the CA algorithm (see section 3). Also, it is expected that running the vehicle with the CA algorithm and the optimal understeer gradient should yield further energy efficiency improvements.

Corresponding to Figure 10a, Figure 10b shows the relative power input increase contours as functions of yaw moment and lateral acceleration. As expected, to achieve the almost neutral steering behavior, the optimum yaw moment is always positive and monotonically increasing with a_Y. Interestingly, the relative power contours are nearly symmetric about the x-axis. Current work is concerned with this aspect.

5 CONCLUSIONS

The experimental work allows the following conclusions:

- Torque vectoring control is effective in improving energy efficiency by reducing power losses associated with the drivetrain and tires.
- The energy efficient CA algorithm allows energy savings typically between 2% and 3% along driving cycles and up to ~4% during cornering conditions with respect to fixed torque distribution strategies.
- The optimal understeer characteristic in terms of energy efficiency is close to the condition of neutral steering for the specific electric vehicle.
- The energy efficient reference cornering response reduces measured input power by up to ~11% for the case study vehicle demonstrator.

REFERENCES

Chen, Y., Wang, J. 2012. Fast and global optimal energy efficient control allocation with applications to overactuated electric ground vehicles. *IEEE Transactions Control Systems Technology* 20(5): 1202–1211.

Chen, Y., Wang, J., 2014. Adaptive energy-efficient control allocation for planar motion control of over-actuated electric ground vehicles. *IEEE Transactions Control Systems Technology* 22(4): 1362–1373.

De Novellis, L., Sorniotti, A., Gruber, P., Ivanov, V., Hoepping, K. 2012. Torque vectoring control for electric vehicles with individually controlled motors: state-of-the-art and future developments. In: *26th International Electric Vehicle Symposium (EVS26), Los Angeles 6-9 May 2012*.

De Novellis, L., Sorniotti, A., Gruber, P. 2013. Optimal wheel torque distribution for a four-wheel-drive fully electric vehicle. *SAE International Journal of Passenger Cars* 6(1): 128–136.

De Novellis, L., Sorniotti, A., Gruber, P., Orus, J., Rodriguez Fortun, J.M., Theunissen, J., De Smet, J. 2015a. Direct yaw moment control actuated through electric drivetrains and friction brakes: theoretical design and experimental assessment. *Mechatronics* 26: 1–15.

De Novellis, L., Sorniotti, A., Gruber, P. 2015b. Driving modes for designing the cornering response of fully electric vehicles with multiple motors. *Mechanical Systems and Signal Processing*, 64-65: 1–15.

Dizqah, A. M., Lenzo, B., Sorniotti, A., Gruber, P., Fallah, S., De Smet, J. 2016. A Fast and Parametric Torque Distribution Strategy for Four-Wheel-Drive Energy Efficient Electric Vehicles. *IEEE Transactions on Industrial Electronics* 63: 4367–4376.

Fujimoto, H., Harada, S. 2015. Model-based range extension control system for electric vehicles with front and rear driving-braking force distributions. *IEEE Transactions on Industrial Electronics* 62(5): 3245–3254.

Jonasson, M., Andreasson, J., Solyom, S., Jacobson, B., Stensson Trigell, A. 2011. Utilization of actuators to improve vehicle stability at the limit: from hydraulic brakes toward electric propulsion. *Journal of Dynamic Systems, Measurement, and Control* 133(5): 051003.

Kang, J., Yoo, J., Yi, K. 2011. Driving control algorithm for maneuverability, lateral stability, and rollover prevention of 4WD electric vehicles with independently driven front and rear wheels. *IEEE Transactions on Vehicular Technology* 60(7): 2987–3001.

Lu, Q., Gentile, P., Tota, A., Sorniotti. A., Gruber, P., Costamagna, F., DeSmet, J. 2016. Enhancing vehicle cornering limit through sideslip and yaw rate control. *Mechanical Systems and Signal Processing* 75: 455–472.

Pennycott, A., De Novellis, L., Sabbatini, A., Gruber, P., Sorniotti A. 2014. Reducing the Motor Power Losses of a Four-Wheel Drive Fully Electric Vehicle via Wheel Torque Allocation. *Proceedings of the Institution of Mechanical Engineers, Part D: Journal of Automobile Engineering* 228(7): 830–839.

Tjønnas, J., Johansen, T.A. 2010. Stabilization of automotive vehicles using active steering and adaptive brake control allocation. *IEEE Transactions Control Systems Technology* 18(3): 545–558.

van Zanten, A., Erhardt, R., Pfaff, G. 1995. VDC, the Vehicle Dynamics Control System of Bosch. *SAE Technical paper* 950749.

Wang, R., Chen, Y., Feng, D., Huang, X., Wang, J. 2011. Development and performance characterization of an electric ground vehicle with independently actuated in-wheel motors, *Journal of Power Sources* 196: 3962–3971.